MODELLING OF THE TOROIDAL ASYMMETRY OF POLOIDAL HALO CURRENTS IN CONDUCTING STRUCTURES

N. POMPHREY, J.M. BIALEK*, W. PARK
Princeton Plasma Physics Laboratory,
Princeton University,
Princeton, New Jersey,
United States of America

ABSTRACT. During plasma disruptions, substantial toroidal and poloidal eddy currents are generated in the vacuum vessel and other plasma facing conducting structures. Eddy currents that conduct charge through paths which close through the plasma periphery are called halo currents, and these can be of substantial magnitude. Of particular concern for tokamak design and operation is the observed toroidal asymmetry of the halo current distribution: such an asymmetric distribution leads to problematic non-uniform forces on the conducting structures. The premise is adopted that the source of toroidal asymmetry is the plasma deformation resulting from the non-linear external kink instability that develops during the current quench phase of a disruption. A simple model is presented of the kinked plasma that allows an analytic calculation of the dependence of the toroidal peaking factor (TPF) on the ratio of the halo current to the total toroidal plasma current, I_h/I_p. Expressions for the TPF as a function of I_h/I_p are derived for $m/n = 2/1$ and $m/n = 1/1$ helical instabilities. The expressions depend on a single parameter, which measures the amplitude of the saturated state of the kink instability. A comparison with disruption data from experiments shows good agreement. Numerical experiments that simulate non-linear external kinks provide guidance on the values expected for the saturated amplitude. It is proposed that a simple plasma halo model is adequate for assessing the engineering impact of asymmetric halo currents, since the force distribution on the conducting structures depends mainly on the 'resistive distribution' of the eddy currents. A brief description is given of an electromagnetics code that calculates the time development of eddy currents in conducting structures, and the code is applied to two halo current disruption scenarios. These are used to emphasize the importance of having an accurate eddy current calculation to correctly estimate the engineering impact of tokamak disruptions.

1. INTRODUCTION

During a plasma disruption, substantial toroidal and poloidal eddy currents are generated in the vacuum vessel and other plasma facing conducting structures. In this article, we concentrate on the poloidal eddy currents.

Eddy currents can be generated by induction, owing to a changing plasma toroidal flux, and by conduction of current from the open field line region of the plasma periphery into solid material conductors such as the first wall or divertor plates (e.g., see the review articles by Gruber and Lackner [1] and by Schuller [2]). 'Halo' current refers to that part of the plasma current which flows in the conducting structure and which has a return path through the plasma (Fig. 1). Having a return path through the plasma has an important consequence, because such a poloidal current, when crossed with the external toroidal magnetic field, can lead to a substantial net force on the conducting structure [3–6].

Halo current magnitudes, I_h, of up to 50% of the pre-disruption plasma current, I_p^0, have been measured in major tokamak experiments [1, 7, 8]. Typical halo current fractions, I_h/I_p^0, are 20%. A particular concern for tokamak design and operation is the observed toroidal asymmetry of the halo current distribution: in some cases, peak to average 'toroidal peaking factors' (TPFs) of 3.0 or more are measured. Figure 2, reproduced from the 1996 paper of Wesley et al. [9], shows disruption data from DIII-D, ASDEX Upgrade, Alcator C-Mod and COMPASS-D. The data show a trend for the TPF to decrease with increasing I_h/I_p^0.

* *Present address*: Skilled Associates, 21 Nassau Court, Skillman, NJ 08558, USA.

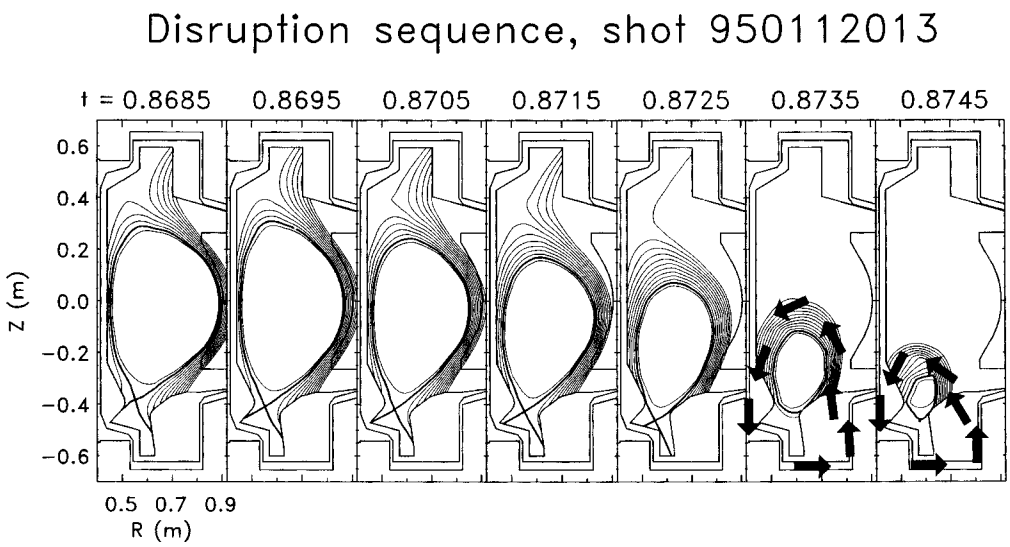

FIG. 1. From Granetz et al. [8]: magnetic flux reconstructions at 1 ms time intervals during a VDE disruption in Alcator C-Mod. The arrows show the poloidal projection of halo current flow from the plasma periphery into the conducting wall, with a return path through the plasma region. A substantial halo current exists primarily during the last two frames.

Clearly, tokamaks such as ITER must be designed to withstand 'worst case' load scenarios in the event of major disruptions. To define such scenarios a priori requires an ability to estimate expected values of the TPFs and halo current fractions. This requires an understanding of the physics of halo currents, and the cause of toroidal peaking.

Toroidal asymmetry of halo current distributions can be due to conductor asymmetries (e.g., built-in vessel asymmetry or vessel distortion during tokamak operation) and/or plasma asymmetries (e.g., plasma deformation due to non-linear development of free boundary instabilities) [6]. Since halo currents are often seen to rotate toroidally, see, for example Ref. [8], the former case can probably be dismissed. In this article, we concentrate on the latter proposition and present a simple analytical model that estimates TPFs for plasmas with helical deformations. The model predicts the dependence of the TPFs on the halo current fraction.

It is easy to see why the non-linear development of an external kink instability leads to toroidally non-uniform halo currents. For example, consider a circular cross-section equilibrium subject to an $m/n = 2/1$ instability. Development of the instability leads to an elliptical deformation of the plasma, as depicted in Fig. 3, and contact with a limiter surface at a local toroidal location ($\phi = 0$ in the figure). The amplitude of the kink is parametrized by the ellipticity, κ. The width of the halo region is denoted by d. The minor radius of the limited plasma is denoted by a. At a given ϕ, depending on the magnitude of κ relative to d/a, all, some or none of the poloidal plasma current is conducted into the wall. Similarly, an $m/n = 1/1$ instability leads to a shifted plasma column and an equivalent scenario for the production of toroidally non-uniform halo currents (Fig. 4). At a given ϕ, depending on the magnitude of the shift, s, of the plasma column relative to the thickness of the plasma halo, all, some or none of the poloidal plasma current is conducted into the wall.

A self-consistent treatment of the plasma evolution and electromagnetic interaction of a three dimensional (3-D) plasma with 3-D conductor regions is not feasible at present. Our goal in this article is to define a simple model of the plasma that is capable of reproducing the observed halo current asymmetries and that can be used as a 'plasma driver' for electromagnetics calculations which calculate 3-D eddy current flow patterns in first wall conducting structures. In calculating the structural impact of asymmetries in tokamak disruptions (e.g., for ITER design), the forces on conducting structures are of primary interest. The poloidal halo currents in the plasma region serve only as a source for eddy currents in the solid conductor regions. Since the currents that flow in the plasma halo are force-free, problematic forces arise only after the eddy current distribution

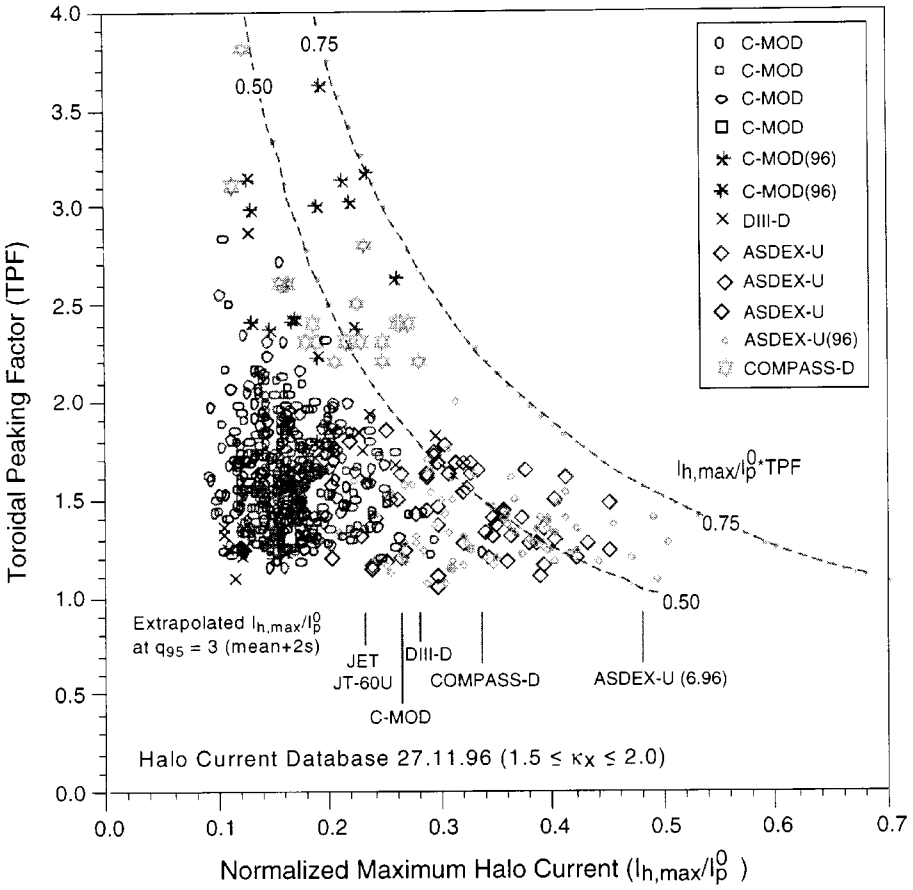

FIG. 2. From Wesley [9]: ITER halo current disruption database of TPFs (peak to toroidally averaged halo current) plotted against maximum halo current fraction of the pre-disruption toroidal plasma current, $I_{\mathrm{h,max}}/I_{\mathrm{p}}^0$. The dashed curves are empirical fits of the form $I_{\mathrm{h,max}}/I_{\mathrm{p}}^0 \times \mathrm{TPF} = c_{\mathrm{fit}}$, with $c_{\mathrm{fit}} = 0.5$ and 0.75.

in the conducting structures evolves towards a resistive distribution. In principle, 3-D plasma simulation codes such as MH3D [10] can be used to calculate the development of non-linear instabilities in fully 3-D toroidal geometry. However, without coupling such codes to a realistic calculation of the eddy currents in 3-D conducting structures, we would be missing the essential ingredient for a realistic force calculation. Past experience with 2-D calculations of halo current forces using the TSC [11] or DINA [12] codes shows that many runs are necessary before a 'worst case scenario' is identified (e.g., the halo temperature and width must be varied, as well as the timing of the current quench with respect to the vertical excursion from the nominal equilibrium position). Each such 2-D simulation is CPU intensive. A single run of a 3-D plasma simulator is substantially slower than that of an equivalent 2-D simulator, therefore performing multiple runs to identify worst case scenarios will lead to an extremely inefficient design tool, given the speed of present day computers. It is necessary to develop a simple plasma driver that can reproduce the essential features of the data observed at present on halo current asymmetries and that can be coupled to detailed electromagnetics codes which calculate eddy currents and disruption loads using realistic models for the conductors. The simplicity of the plasma driver should allow scoping studies to be performed.

In Section 2, we define a simple plasma model for a helically deformed plasma that allows an analytic calculation of the toroidal peaking factors and their dependence on halo current fraction, $I_{\mathrm{h}}/I_{\mathrm{p}}$. Results are shown in Section 3 for both $m/n = 2/1$ and $m/n = 1/1$ instabilities. For each mode, the dependence of TPF on $I_{\mathrm{h}}/I_{\mathrm{p}}$ is on a single parameter that determines the amplitude of the saturated state of the non-linear instability. For the $m/n = 2/1$ instability,

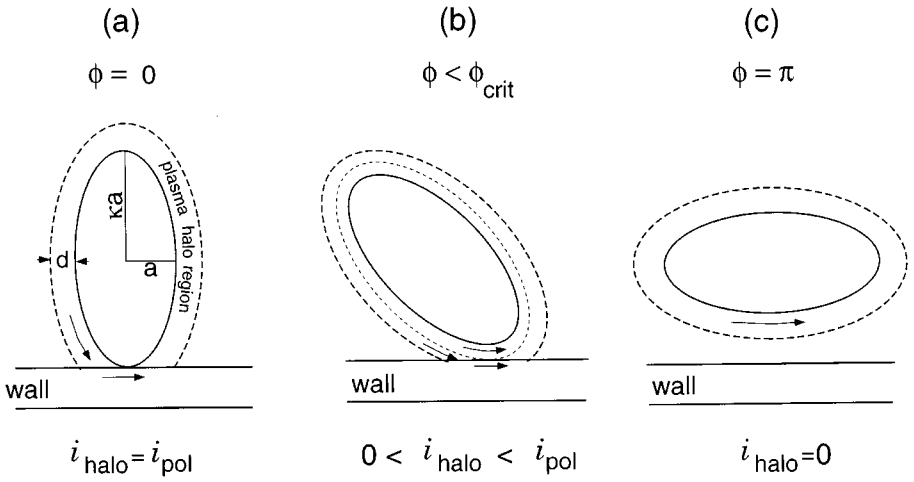

FIG. 3. Elliptical deformation of a plasma resulting from an $m/n = 2/1$ helical kink instability will lead to a toroidally asymmetric halo current. The poloidal cross-section of the kinked plasma is shown at three different toroidal angles, ϕ. Poloidal current flow is depicted by arrows drawn in the plasma periphery and conducting wall regions. At a given ϕ, depending on the amplitude of the kink (parametrized by the ellipticity κ) and the relative thickness, d/a, of the plasma halo region, all, some or none of the poloidal halo current in the plasma is conducted into the wall.

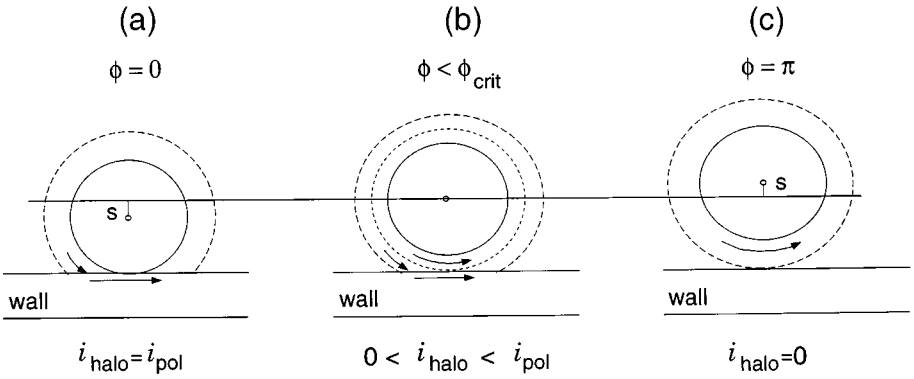

FIG. 4. Halo current can also arise owing to a column shift of the plasma resulting from an $m/n = 1/1$ helical kink instability. At a given toroidal angle, ϕ, depending on the magnitude of the column shift, s, and relative thickness, d/a, of the plasma halo region, all, some or none of the poloidal halo current in the plasma is conducted into the wall.

this parameter is the perturbed ellipticity, κ. For the $m/n = 1/1$ instability, the parameter is the normalized column shift, s/a. The simple model reproduces the hyperbolic-like decrease in the TPF as a function of the I_h/I_p observed in the experimental data. In addition, the magnitudes of the predicted TPFs are in agreement with the experimental data for 'sensible' values of κ and s/a: TPF values exceeding 2.0 are obtained for halo current fractions of 20% for $\kappa \approx 2.0$ or for $s/a \approx 0.2$.

To use the simple plasma model as a tool for machine design, we need to know the values to assign to the model parameters κ or s/a. In particular, we would like to know the maximum likely values for these parameters. Since this information does not exist in the available experimental database, numerical simulations must provide guidance. In Section 4, we describe some numerical simulations of the non-linear development of $m/n = 2/1$ external kink modes. Depending on the equilibrium profile

parameters and relative separation distance between the conducting wall and the plasma, elliptical surface deformations with κ up to 3.0 have been calculated. These calculations have assumed helical symmetry and infinite aspect ratio. There are prospects, however, of extending the calculations to full 3-D geometry at finite aspect ratio.

From the point of view of tokamak machine design, we are not so much interested in halo currents and their toroidal asymmetries as we are in calculating the magnitude and direction of the forces on conductors. To determine a load on a conducting structure requires the calculation of a (time dependent) eddy current distribution. The instant that a force-free plasma source distribution of halo current is applied to a conductor, the eddy current in the conductor is also force-free; the spatial distribution of the eddy current is the same as that of the plasma source. After an appropriately defined L/R time of the conductor, the eddy current distribution relaxes to a 'resistive distribution' that depends critically on the available conducting paths in the conductor. The resistive distribution may depend only weakly on the source distribution. Since one is interested in the forces on the conductors, the resistive distribution is of primary concern, not the source distribution.

In Section 5, we present a brief description of an electromagnetics code that calculates the time development of eddy currents in conducting structures and that allows the user to include sources and sinks of halo current. Two halo eddy current calculations are presented that illustrate the importance of being able to correctly calculate the eddy current distribution. In the first calculation, the kinked plasma halo current model of Section 2 is used as a driver for a detailed electromagnetics calculation of eddy currents on a conducting plate. The disruption scenario assumes that a vertical displacement episode (VDE), accompanied by an $m/n = 1/1$ kink instability, has allowed an aspect ratio 3.0 disrupting plasma to come into contact with a horizontal conducting plate. It is shown that a detailed calculation of the eddy current distribution leads to a much more complicated force distribution than the one that would be predicted if a naïve eddy current model was used which assumes that the current paths between the plasma halo sources and the sinks are purely poloidal. In fact, some areas of the plate experience forces opposite in direction to those predicted by the naïve model. The second example is a model of a radial disruption in NSTX, a low aspect ratio ($A = 1.26$) 1.0 MA tokamak device currently being built in the United States of America. For this example, it is assumed that a radial disruption has led to contact of the plasma with the central stack casing. In spite of an imposed toroidal asymmetry of the halo current source and sink distribution corresponding to a TPF of 2.0, the calculated resistive distribution of currents in the central stack shows a remarkable lack of asymmetry. In particular, midway between the sources and the sinks, the TPF is only 1.05. Both examples presented in this section show the importance of considering forces and associated TPFs as derived quantities.

Conclusions are presented in Section 6.

2. MODEL OF KINKED PLASMA, AND DERIVATION OF TOROIDAL PEAKING FACTORS

2.1. Kink instability with $m/n = 2/1$

We assume that a disruption has been triggered by an $m/n = 2/1$ kink instability. The mode develops non-linearly, leading to a deformation of the plasma surface and edge region. The initial development is rapid, on an MHD (Alfvén) time-scale. Nearby conductors (such as passive stabilizers for vertical control of elongated plasmas) behave electromagnetically as perfect conductors. The kink saturates on the fast time-scale with a finite amplitude parametrized by the kink elongation, κ (e.g., Fig. 3(a)). A loss in plasma beta leads to a loss of position control (e.g., a VDE) and to limiter contact between the plasma and a solid conductor region. The solid conductors now behave as finite resistivity conductors, allowing plasma motion and further development of the kink instability on the L/R time-scale of the conductors.

We treat the plasma perturbatively as a helical distortion of a 1-D axisymmetric system. The 'flux co-ordinate' ρ labels the flux surfaces, with $\rho = 1$ denoting the limiter surface to the confined plasma region, and $\rho = \rho_{\mathrm{h}}$ labelling the edge of the plasma halo region of open field lines that intersect the wall. In the confined plasma region we assume a parametrization of the flux surfaces consistent with a constant current density plasma, and assume a large aspect ratio approximation. Thus, the plasma and plasma halo region co-ordinate surfaces are represented by

$$X = R + r\cos\theta, \qquad Z = r\sin\theta \tag{1a,b}$$

$$r^2 = a^2\,\frac{\rho}{2}[(\kappa^2+1) - (\kappa^2-1)\cos(2\theta - \phi)] \tag{2}$$

where

$$0 < \rho < \rho_{\mathrm{h}} = (1 + d/a)^2. \tag{3}$$

The relevant parameters of the model are shown in Fig. 5, which shows the co-ordinate surfaces corresponding to $\rho = 1$ and $\rho = \rho_\mathrm{h}$ for toroidal angle $\phi = 0$. The midplane minor radius of the limited plasma is $r = a$, and the midplane width of the halo is $\delta r = d$. The elongation of the kinked plasma, denoted by κ, represents an elongation relative to a circular equilibrium. To interpret the parameter κ for non-circular equilibria, we define κ as $(1 + \Delta a/a)/(1 - \Delta a/a)$, where Δa is the midplane deformation of the plasma minor radius. For simplicity, we assume that the solid conductor in contact with the plasma is a planar surface at constant $Z = Z_\mathrm{wall}$.

In the plasma halo region ($1 < \rho < \rho_\mathrm{h}$), we assume that the plasma is force-free with $\boldsymbol{J} = \lambda \boldsymbol{B}$, and λ a constant. The toroidal magnetic field is written as

$$\boldsymbol{B}_\mathrm{t} = g \boldsymbol{\nabla} \phi \tag{4}$$

where $g(\rho) = g_0 + \lambda\rho$ and g_0 is a constant. If there is no toroidal asymmetry, the poloidal current in the plasma halo region, I_pol, is

$$I_\mathrm{pol} = \int_0^{2\pi} \mathrm{d}\phi \, i_\mathrm{pol} \tag{5}$$

where the poloidal halo current density, i_pol, is given by

$$i_\mathrm{pol} = \int_1^{\rho_\mathrm{h}} \mathrm{d}\rho \, \mathcal{J} J^\theta \tag{6}$$

$$= g(1) - g(\rho_\mathrm{h}), \qquad \text{independent of } \phi. \tag{7}$$

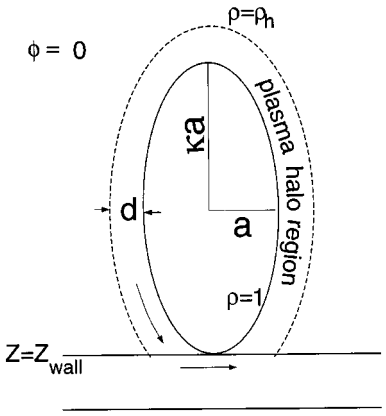

FIG. 5. Geometric parameters relevant to the calculation of toroidal peaking factors for the $m/n = 2/1$ kink instability model are identified: a is the minor radius of the kinked plasma, κ is its elongation and d is the thickness of the plasma halo region. The halo extends from the limiter flux value $\rho = 1$ to a halo edge value of $\rho = \rho_\mathrm{h} = (1 + d/a)^2$. The conducting wall is assumed to be planar and axisymmetric, and located at $Z = Z_\mathrm{wall}$.

In Eq. (6), $\mathcal{J}$ is the Jacobian of the transformation from cylindrical co-ordinates (X, Z, ϕ) to flux co-ordinates (ρ, θ, ϕ). J^θ is the contravariant poloidal component of the current density, i.e. $J^\theta = \boldsymbol{J} \cdot \boldsymbol{\nabla}\theta$. For this axisymmetric case all of the plasma poloidal current is conducted into the wall region, therefore the halo current entering the wall is

$$I_\mathrm{h} = I_\mathrm{pol}. \tag{8}$$

In the case of the toroidally asymmetric model (Eqs (1) to (3)), however, at each ϕ there is a critical $\rho = \rho_\mathrm{w}(\phi)$ such that only for $1 < \rho_\mathrm{w}(\phi) < \rho < \rho_\mathrm{h}$ is poloidal current conducted into the wall. A typical situation is shown in Fig. 6, thus,

$$i_\mathrm{halo}(\phi) = \int_{\rho_\mathrm{w}(\phi)}^{\rho_\mathrm{h}} \mathrm{d}\rho \, \mathcal{J} J^\theta \tag{9}$$

$$= g(\rho_\mathrm{w}(\phi)) - g(\rho_\mathrm{h}). \tag{10}$$

To determine $\rho_\mathrm{w}(\phi)$, we apply the tangency condition

$$\left.\frac{\partial Z}{\partial \theta}\right|_{Z = Z_\mathrm{wall}} = 0 \tag{11}$$

which yields

$$\rho_\mathrm{w}(\phi) = \frac{\kappa^2}{\sin^2\phi/2 + \kappa^2 \cos^2\phi/2}. \tag{12}$$

Thus,

$$i_\mathrm{halo}(\phi) = \lambda \left[\frac{\kappa^2}{\sin^2\phi/2 + \kappa^2 \cos^2\phi/2} - \left(1 + \frac{d}{a}\right)^2 \right] \tag{13a}$$

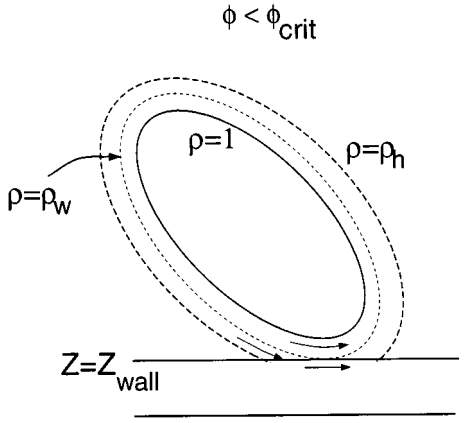

FIG. 6. Poloidal cross-section of an $m/n = 2/1$ kinked plasma sketched at some intermediate ϕ such that poloidal plasma current is conducted into the wall for $\rho_\mathrm{w}(\phi) < \rho < \rho_\mathrm{h}$.

if $\rho_w(\phi) \geq \rho_h$ and

$$i_{halo}(\phi) = 0 \tag{13b}$$

if $\rho_w(\phi) < \rho_h$. We define the TPF as

$$\mathrm{TPF} = \frac{i_{halo}^{max}}{\langle i_{halo} \rangle} \tag{14}$$

where

$$\langle i_{halo} \rangle \equiv \frac{1}{2\pi} \int_0^{2\pi} d\phi \, i_{halo}(\phi) \tag{15}$$

is the toroidally averaged halo current flowing into the conducting wall. Considering, first, the case where $\kappa < 1 + d/a$,

$$\langle i_{halo} \rangle = \frac{1}{2\pi} \int_0^{2\pi} \lambda \left(\frac{\kappa^2}{\sin^2\phi/2 + \kappa^2 \cos^2\phi/2} - \rho_h \right) d\phi \tag{16}$$

i.e. the full range of ϕ is included in the integration. The right hand side of Eq. (16) is easily evaluated and yields

$$\langle i_{halo} \rangle = \lambda(\kappa - \rho_h). \tag{17}$$

In the case of $\kappa > 1 + d/a$, the algebra is complicated by the fact that there is a critical angle, $\phi_{crit} < \pi$, such that poloidal current enters the wall only for $0 < \phi < \phi_{crit}$ and for $\pi - \phi_{crit} < \phi < \pi$. (This situation is illustrated in Fig. 7.) The value of ϕ_{crit} is determined from Eq. (12) by setting the left hand side equal to $\rho_h = (1 + d/a)^2$. This yields

$$\tan \frac{\phi_{crit}}{2} = \kappa T \tag{18}$$

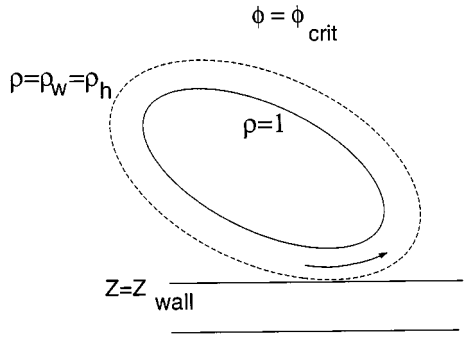

FIG. 7. Poloidal cross-section of an $m/n = 2/1$ kinked plasma is shown at $\phi = \phi_{crit} < \pi$, where ϕ_{crit} is the critical toroidal angle corresponding to tangency of the $\rho = \rho_h$ surface with the wall. If $\phi > \phi_{crit}$, no poloidal plasma current is conducted into the wall. A ϕ_{crit} also exists for $\phi > \pi$.

where

$$T = \left(\frac{\rho_h - 1}{\kappa^2 - \rho_h} \right)^{1/2}. \tag{19}$$

Then, for the toroidally averaged halo current in the case of $\kappa < 1 + d/a$, we obtain

$$\langle i_{halo} \rangle = \frac{1}{2\pi} 2 \int_0^{\phi_{crit}} \lambda \left(\frac{\kappa^2}{\sin^2\phi/2 + \kappa^2 \cos^2\phi/2} - \rho_h \right) d\phi \tag{20}$$

$$= \frac{\lambda}{\pi/2} \left(\kappa \tan^{-1} T - \rho_h \tan^{-1} \kappa T \right). \tag{21}$$

The peak value of the halo current is $i_{halo}^{max} = i_{halo}(\phi = 0) = \lambda(1 - \rho_h)$. Therefore, the TPF for the $m/n = 2/1$ plasma halo model is

$$\mathrm{TPF}_{21} = \frac{\rho_h - 1}{\rho_h - \kappa} \tag{22a}$$

for $\kappa < 1 + d/a$ and

$$\mathrm{TPF}_{21} = \frac{\rho_h - 1}{2\pi^{-1}(\rho_h \tan^{-1} \kappa T - \kappa \tan^{-1} T)} \tag{22b}$$

for $\kappa > 1 + d/a$. The TPF is seen to be a function of d/a, the relative thickness of the plasma halo region, and of κ, the kink deformation.

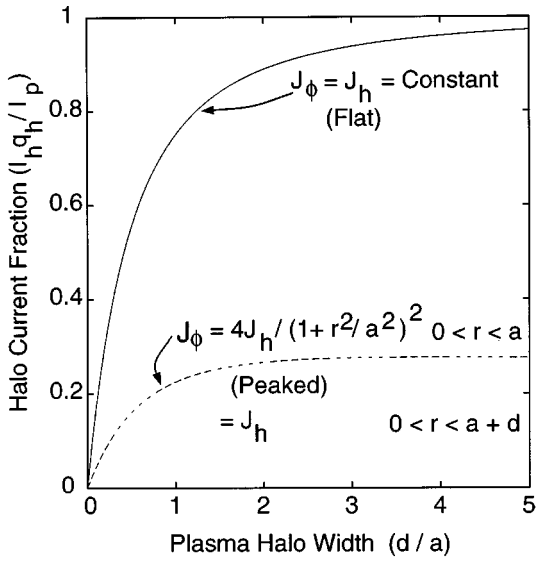

FIG. 8. Halo current fraction, $I_h q_h / I_p$, plotted as a function of plasma halo width, d/a, for a flat current model (corresponding to $q = q_h$ everywhere in the region $0 < r < a + d$) and for a peaked current model (where $q = q_h(1 + r^2/a^2)/2$ in the region $0 < r < a$ and $q = q_h$ in the region $a < r < a + d$). For the peaked profile model, maximum halo current fractions are less than 30%.

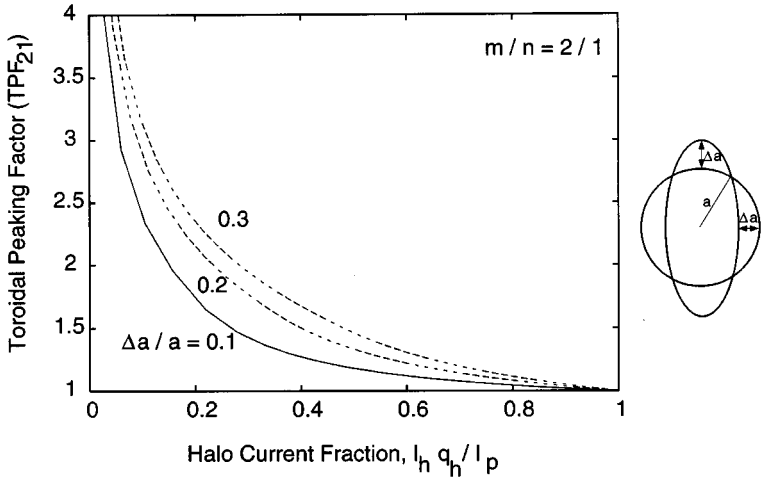

FIG. 9. Plot of the TPF for the $m/n = 2/1$ deformed plasma kink model, TPF_{21}, as a function of halo current fraction, $I_\mathrm{h}q_\mathrm{h}/I_\mathrm{p}$. Each curve is labelled by the surface deformation, $\Delta a/a$.

A final step is to relate d/a to the halo current fraction, $I_\mathrm{h}/I_\mathrm{p}$. Assuming a constant current density, with $q = q_\mathrm{h} = \text{const}$ everywhere, one easily calculates

$$I_\mathrm{h}q_\mathrm{h}/I_\mathrm{p} = 1 - 1/\rho_\mathrm{h}. \tag{23}$$

Thus, Eqs (22a, b) can be used to generate curves of toroidal peaking factor versus halo current fraction, parametrized by the kink elongation, κ.

It is interesting to compare the halo current fractions predicted by Eq. (23) with the values predicted using a peaked current profile, such as $q = q_\mathrm{h}(1 + r^2/a^2)/2$ within the limited region $0 < r < a$, and $q = q_\mathrm{h} = \text{const}$ within the halo $a < r < a+d$. Figure 8 shows the comparison, and makes it clear that in order to achieve the substantial (>50%) halo current fractions observed in experiments (e.g., Fig. 2), it is necessary to assume a flat profile.

2.2. Kink instability with $m/n = 1/1$

The calculation of toroidal peaking factors for the case of halo current asymmetries driven by an $m/n = 1/1$ kink mode is very similar to the description given above for the $m/n = 2/1$ model, therefore we will omit the details. The co-ordinate surfaces for the perturbed plasma and plasma halo regions are given by the representation

$$X - R + s\cos\phi = \rho^{1/2}a\cos\theta \tag{24}$$

$$Z + s\sin\phi = \rho^{1/2}a\sin\theta \tag{25}$$

where the column shift, s, parametrizes the amplitude of the 1/1 kink. Expressions for the toroidal peaking factor as a function of s/a and the relative thickness of the plasma halo region, d/a, are derived to be

$$\mathrm{TPF}_{11} = \left(1 - \frac{s}{2d}\,\frac{(4a+3s)}{(2a+3d)}\right)^{-1} \tag{26a}$$

for $s \le d/2$ and

$$\mathrm{TPF}_{11} = \frac{\lambda}{\pi}\left\{\phi_\mathrm{crit}\left[\left(1+\frac{s}{a}\right)^2 + \frac{1}{2}\left(\frac{s}{a}\right)^2 - \rho_\mathrm{h}\right] + \frac{1}{4}\left(\frac{s}{a}\right)^2\sin 2\phi_\mathrm{crit} - 2\left(1+\frac{s}{a}\right)\frac{s}{a}\sin\phi_\mathrm{crit}\right\} \tag{26b}$$

for $s > d/2$, where

$$\tan\phi_\mathrm{crit} = \frac{[d(2s-d)]^{1/2}}{s-d}. \tag{27}$$

Equations (26a, b) and (27), together with Eq. (23), can be used to generate curves of toroidal peaking factor versus halo current fraction, parametrized by the kink shift, s.

3. RESULTS

Plots of TPF versus halo current fraction, $I_\mathrm{h}q_\mathrm{h}/I_\mathrm{p}$, are shown in Figs 9 and 10 for both the $m/n = 2/1$ model and the $m/n = 1/1$ model. In the case of $m/n = 2/1$, each curve is labelled by the surface deformation $\Delta a/a$, which is related to the perturbed elongation by $\kappa = (1 + \Delta a/a)/(1 - \Delta a/a)$. In the case of $m/n = 1/1$, each curve is labelled by the

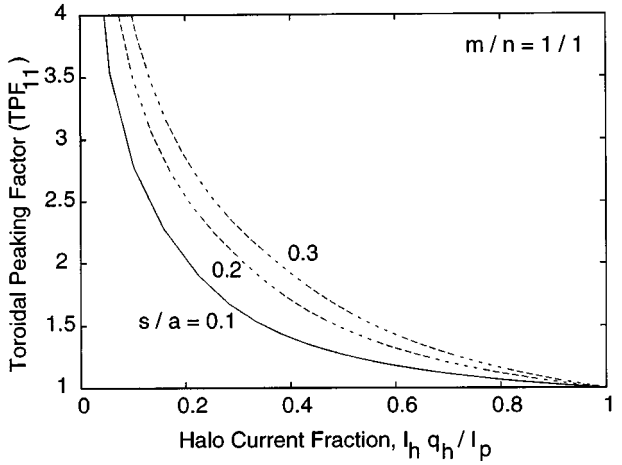

FIG. 10. Plot of the TPF for the $m/n = 1/1$ deformed plasma kink model, TPF_{11}, as a function of the halo current fraction, $I_\mathrm{h}q_\mathrm{h}/I_\mathrm{p}$. Each curve is labelled by the plasma column shift, s/a.

column shift normalized by the equilibrium radius, i.e. s/a. We note that the simple model reproduces the decrease in TPF with increasing $I_\mathrm{h}/I_\mathrm{p}$ observed in the experimental data (Fig. 2). The magnitudes of the predicted TPF values are in agreement with the experimental data for reasonable values of κ and s/a (see results of Section 4 for why these values are 'reasonable'): for example, TPF values exceeding 2.0 are obtained for halo current fractions of 20% for $\Delta a/a \approx 0.2$ or for $s/a \approx 0.2$.

3.1. Discussion

The simple model described in the previous two sections predicts a dependence of TPF on halo current fraction that is similar to that of the observed experimental data. The quantitative predictions of the model depend only on the assumed values for the single parameters $\Delta a/a$ or s/a. These parameters are a measure of the amplitude of the non-linear external kink responsible for the halo current asymmetry. When comparing the model results with the experimental database, we must bear in mind that the data in Fig. 2 use the predisruption plasma current, I_p^0, as the denominator in the definition of halo current fraction, whereas the model and its results in Figs 9 and 10 use the instantaneous current, I_p. Although an empirical fit to the database is presented in Fig. 2 in the form of curves of $I_{\mathrm{h,max}}/I_\mathrm{p}^0 \times \mathrm{TPF} = c_\mathrm{fit}$, with $c_\mathrm{fit} = 0.5$ and 0.75, the comparison with the predictive curves in Figs 9 and 10 is problematic, since the relationship between the value of I_p at the time for which I_h is a maximum and the value of I_p^0 depends on details of the time dependence of the plasma temperature and inductance during the current quench. This relationship may differ substantially from machine to machine. Since the ratio $I_\mathrm{h}/I_\mathrm{p}$ is fundamental, rather than $I_\mathrm{h}/I_\mathrm{p}^0$, one procedure for scaling the existing experimental data to a tokamak such as ITER would be to decide on the 'largest likely value' of the parameter $\Delta a/a$ or s/a, then to transform from $I_\mathrm{h}/I_\mathrm{p}$ to $I_\mathrm{h}/I_\mathrm{p}^0$ using an ITER-specific model that predicts the time dependence of the quenching current, $I_\mathrm{p}(t)$.

4. NUMERICAL SIMULATION OF NON-LINEAR EXTERNAL KINKS

In this section, we briefly describe some attempts at the numerical simulation of non-linear external kinks. The focus here is on the question: What are sensible bounding values for the model parameters ($\Delta a/a$ or s/a) that fix the dependence of TPF on halo current fraction? Ideally, we should appeal to experimental data to provide values. Unfortunately, these experimental data do not at present exist. Therefore, we are forced to turn to numerical simulation to provide guidance. To answer the question does not require detailed simulations of disruptions, merely the determination of the amplitude of the saturated states of non-linear kink instabilities.

4.1. Previous studies

Early published studies include those by Sykes and Wesson [13] and by Dnestrovskii and Kostomarov [14]. Sykes and Wesson calculated self-consistent solutions of the helical Grad–Shafranov equation at infinite aspect ratio. Their initial equilibrium is a circular cross-section plasma with an ohmic toroidal current profile of the form $J_\phi = J_0(1-r^2/a^2)^{q_\mathrm{edge}/q_\mathrm{axis}-1}$, and q_edge chosen so that the equilibrium is linearly unstable to an external kink mode of a chosen helicity. A perfectly conducting wall is assumed at some radius $r_\mathrm{w} > a$, and solutions to the helical equilibrium equations determined for a given wall radius. With $m/n = 2/1$, $r_\mathrm{w}/a = 1.2$, $q_\mathrm{axis} = 1.0$ and $q_\mathrm{edge} \approx 2.0$, surface deformations $\Delta a/a \sim 0.3$ were found (Fig. 3(d) of Ref. [13]). The deformation decreases monotonically as q_edge is lowered. Similar deformation values were calculated by Dnestrovskii and Kostomarov (Fig. 7 of Ref. [14]) using an initial value code that integrates the reduced MHD equations. During the non-linear evolution of the kink mode, the resistivity profile, $\eta(\psi)$, was assumed to be a fixed function of the

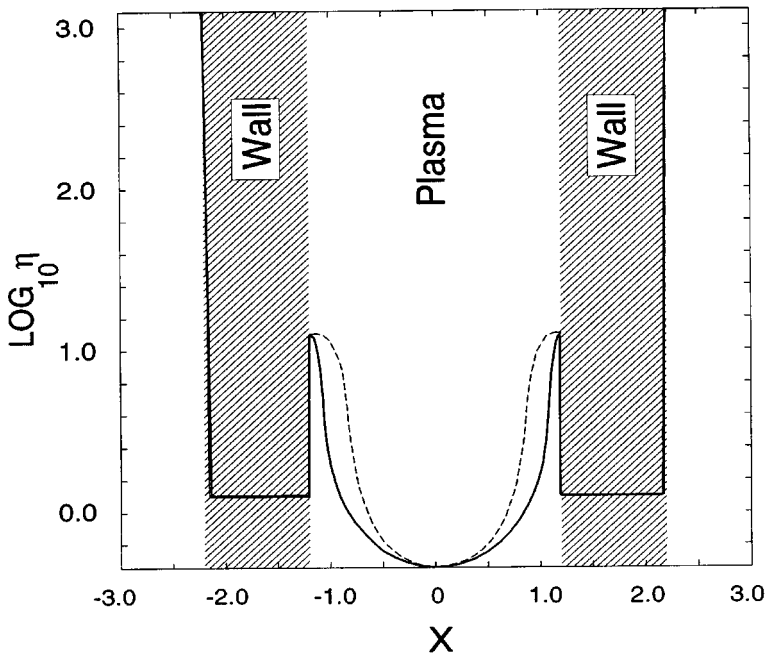

FIG. 11. Simulation of a non-linear external kink with the MH3D code: plot of resistivity profile (logarithmic scale) at toroidal angle $\phi = 0$. The units of length are chosen such that the minor radius of the initial free boundary plasma equilibrium is $r = a = 1.0$. The solid curve is the resistivity profile plotted along the midplane (X axis at $Z = 0$); the dashed curve is the corresponding plot along the Z axis at $X = 0$. The difference between the curves reflects the fact that the plasma cross-section is horizontally elongated by the kink perturbation. A thick conducting wall of unit thickness extends from a radius of 1.2. Perfectly conducting boundary conditions are applied at a radius of $3.0a$.

helical flux, ψ, and constant in time over a given flux surface. The 'vacuum' region assumes $\eta = \text{const}$, and is sufficiently resistive that current flow is negligible. A rapid transition of η from the vacuum to the plasma region (where $\eta_\text{p} \sim 10^{-4}\eta_\text{vac}$) simulates the free boundary plasma. Assuming a perfectly conducting wall at $r_\text{w}/a = 1.5$, surface deformations of $\Delta a/a$ up to 0.5 were calculated.

4.2. Simulation of non-linear external kinks using the MH3D code

Recently, we have used the MH3D code to follow the non-linear development of external kink modes and their interaction with conducting walls. MH3D is a fully non-linear, resistive, compressible 3-D toroidal initial value code that has been used extensively for studying the resistive stability of internal modes in toroidal plasmas [10, 15], and also the stabilization of external kink modes influenced by toroidal plasma rotation [16]. The non-linear kink simulations using MH3D differ from those of Dnestrovskii and Kostomarov reported above, in two main respects: First, in the MH3D simulations the plasma resistivity is evolved in time by choosing $\eta \propto p^{-3/2}$. The MHD constraint $\mathrm{d}\eta/\mathrm{d}t = 0$ is therefore automatically satisfied through the correct evolution of the pressure equation, as described in Ref. [10]. Second, a resistive wall is included in the calculation. Neither of these differences with Dnestrovskii's work is essential to the results presented below.

The initial plasma is axisymmetric, has a circular cross-section, is chosen to have a large (effectively infinite) aspect ratio, and has zero beta. The initial plasma resistivity profile is related to the current profile through the ohmic constraint $\eta(r)J_\phi(r) = \eta_0 J_0$ for $0 < r < a$. The current profile has a Sykes–Wesson form, but with a constant shift required to make the 'vacuum' resistivity finite:

$$J_\phi = J_1 + (J_0 - J_1)(1 - r^2/a^2).$$

For a narrow transition region beyond $r = a$, we make a smooth transition of $\eta(r)$ to the vacuum region where $\eta(r) = \eta_{\rm vac} = {\rm const}$. We choose parameters such that $q_{\rm edge} = 1.75$, $q_{\rm edge}/q_0 = 2.0$, and $\eta_{\rm p} \sim 10^{-1.2}\eta_{\rm vac}$. A (thick) finitely conducting wall is placed at a radius of $r_{\rm w}/a = 1.2$. The wall was chosen to be artificially thick so that we could easily resolve the halo eddy current patterns (not presented here). The conducting wall resistivity is a factor of 10 smaller than the resistivity of the plasma edge and is comparable to the resistivity of the plasma core. Slip velocity boundary conditions are imposed at the inner radius of the wall. Beyond the conducting wall is a true vacuum region, which extends to a perfectly conducting computational boundary at a radius of $3.0a$.

The plasma is perturbed linearly by an $m/n = 2/1$ perturbation, and a linear eigenfunction determined. This is used as an initial condition for the non-linear computation. Helical symmetry is enforced throughout. The computations proceed until the amplitude of the external kink saturates on the ideal time-scale. (The mode continues to grow on the slow L/R time-scale of the resistive wall.)

Figures 11 and 12 show profile plots of the calculated saturated state: Fig. 11 shows the resistivity profile and Fig. 12 shows two contour plots of the pressure profile that make clear the helical distortion of the plasma. The measured ellipticity of the final state for this case with a wall at $r_{\rm w}/a = 1.2$ is a modest $\kappa = 1.3$, which gives $\Delta a/a = 0.13$.

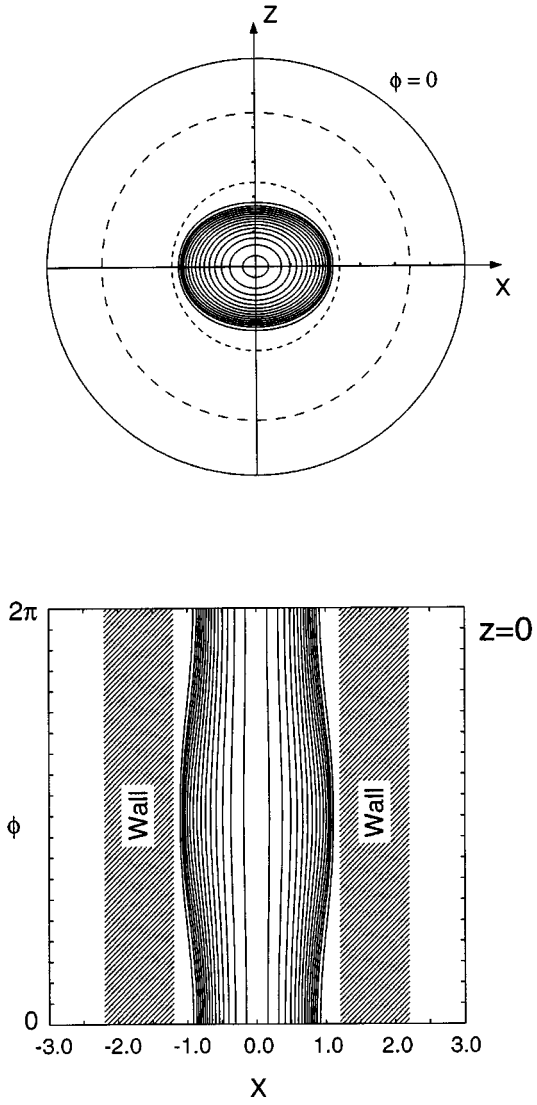

FIG. 12. Non-linear external kink simulation with the MH3D code. Top: contours of plasma pressure on the poloidal plane at toroidal angle $\phi = 0$. The two dashed circles show the inner and outer boundaries of the finite resistivity conducting wall. The outermost solid circle corresponds to the computational boundary, which is a perfectly conducting wall. The elliptical deformation of the plasma cross-section from the initial circle corresponds to $\Delta a/a = 0.13$. Bottom: contours of plasma pressure on the $Z = 0$ plane. The helical deformation of the pressure contours is readily apparent.

4.3. Discussion

Numerical simulation can provide information about the deformation parameters that determine the curves of toroidal peaking factor versus halo current fraction. A number of such calculations have been performed by various authors using helical equilibrium solvers and initial value MHD codes. All calculations to date have concentrated on the $m/n = 2/1$ helical kink instability. Using a limited set of equilibrium profile parameters and separation distances of the conducting wall from the plasma, elliptical surface deformations of $\Delta a/a$ up to 0.50 have been calculated. Limiting ourselves to wall separations of order $r_{\rm w}/a = 1.2$, more realistic for shaped tokamak design, the maximum surface deformation so far calculated is $\Delta a/a \approx 0.3$. None of the calculations have been carried out in full 3-D and at finite aspect ratio. We are planning to do such calculations using the MH3D code after completing a modification of the co-ordinate representation used by the code from Fourier to configuration space, including an unstructured mesh capability.

5. CALCULATION OF HALO EDDY CURRENTS AND DISRUPTION LOADS

In the design and analysis of plasma facing conducting structures, it is important to identify 'worst case' load scenarios. Disruptions may include halo currents. The sum of halo currents and inductively induced eddy currents determines the mechanical loads that the design must handle. The distribution of these currents is time dependent. Initially the spatial distribution of the eddy current is strongly dependent on the current source distribution (an 'inductive solution'). For longer times, however, the eddy current distribution accommodates the geometry and conductivity of the conducting structure and, while decaying in magnitude, develops a spatial distribution (the 'resistive distribution') that depends only weakly on the initial source distribution. Clearly, in order to determine a worst case load scenario, it is crucial to have a good model of the conducting structure. This necessarily means a 3-D model.

Experience with coupling 2-D halo current sources (e.g., provided by TSC) with 3-D eddy current modelling codes, such as SPARK [17], has shown that many plasma disruption scenarios must be analysed before a worst case load scenario is identified. For example, varying the temperature and width of the halo and the timing of the current quench relative to the plasma drift during a VDE can have a significant impact on the magnitude of axisymmetric halo currents. Each 2-D plasma simulation is time consuming, requiring typically several CRAY-II CPU hours. Because of the greater complexity of 3-D free boundary time dependent plasma simulations (e.g., using MH3D) compared with 2-D simulations, it is clear that it will be many years before such 3-D plasma physics codes can be coupled to engineering design analysis codes to obtain a hybrid code that will be useful as a design tool for machines such as ITER: the turn-around calculation time for such a hybrid code would be too slow to be useful. It is our belief that in order to address important engineering issues of machine design, it is more important for the eddy current calculator to be accurate than it is for the plasma driver to be accurate. Therefore, we wish to promote the use of simple 3-D plasma halo drivers (such as the one described in this article) and their coupling to electromagnetics codes which calculate eddy currents and disruption loads on realistic models of tokamak conductors. The simplicity of the plasma drivers will allow parameter scans to be performed. We have recently investigated the effects of our proposed asymmetric plasma model in a collection of simple engineering models. In order to understand the effects of the plasma asymmetries, the engineering models were chosen to be symmetric.

5.1. Eddy current calculations

An eddy current calculation was developed that has two important features:

(a) Only the conducting structure is modelled,
(b) Current conservation is explicit in the formulation.

Feature (a) is a common approach in eddy current codes; the flux change produced by the plasma is specified in place of the plasma dynamics (frequently with help from codes similar to TSC). The second feature is somewhat unique. By explicitly enforcing current conservation, the engineer has the opportunity to introduce regions where (halo) currents explicitly enter or leave the model. The consistent combination of these two effects allows the calculation of forces resulting from disruptions that include halo currents.

For discussion purposes, it is useful to think of this eddy current calculation as a detailed 'branch network' model commonly used by electrical engineers. The complete problem can be summarized by the following equations:

$$\begin{pmatrix} \mathbf{L} & \mathbf{0} \\ \mathbf{0} & \mathbf{0} \end{pmatrix} \begin{pmatrix} \dot{\boldsymbol{I}} \\ \dot{\boldsymbol{V}} \end{pmatrix} + \begin{pmatrix} \mathbf{R} & \mathbf{A} \\ \mathbf{A}^{\mathrm{t}} & \mathbf{0} \end{pmatrix} \begin{pmatrix} \boldsymbol{I} \\ \boldsymbol{V} \end{pmatrix} = \begin{pmatrix} \boldsymbol{b} \\ \boldsymbol{f} \end{pmatrix}. \quad (28)$$

Here the unknown variables are 'branch currents', $\boldsymbol{I}$, and nodal voltages, $\boldsymbol{V}$. The (dense) branch to branch inductance matrix is denoted by $\mathbf{L}$, and $\mathbf{R}$ is the branch resistance matrix (usually diagonal). All the geometry of the model is embedded in the inductance matrix and in the branch node incidence matrix $\mathbf{A}$ (not necessarily square). The top equations in (28) correspond to a statement of the voltage drop in the branches of the model; the $\boldsymbol{b}$ on the top right hand side contains the forcing voltages (inductive or otherwise). The bottom equations in (28) correspond to current conservation at every 'node' in the problem; the right hand side $\boldsymbol{f}$ contains a zero value when current is conserved at a node or a non-zero value when current is injected or extracted locally from the model. The calculation of $\mathbf{L}$ is done using volumetric current distributions for the 'shape functions' used in each of the elementary elements constituting the complete model. The terms on the right hand side are

usually functions of time allowing the description of transient events.

In the special case where the resistive limit is desired, some simplification is possible. If we consider the very restrictive situation when all the forcing voltages are zero (i.e., $\boldsymbol{b} = \mathbf{0}$), then a substantial simplification is possible. This situation is represented by the following equations:

$$-\mathbf{A}^{\mathrm{t}}\mathbf{R}^{-1}\mathbf{A}\boldsymbol{V} = \boldsymbol{f}. \tag{29}$$

Once the nodal voltages are obtained, the branch currents may be calculated using the side calculation $\boldsymbol{I} = -\mathbf{R}^{-1}\mathbf{A}\boldsymbol{V}$. This very restricted resistive distribution formulation is the same as a conductance matrix formulation frequently used in electrical engineering (the matrix $-\mathbf{A}^{\mathrm{t}}\mathbf{R}^{-1}\mathbf{A}$ is the conductance matrix). In either case, once the branch currents are available, one can calculate the distribution of forces by doing the appropriate integrations and cross-products with the total magnetic field.

If we use Eq. (28) for a plasma disruption without halo currents (i.e. only specifying a flux change), we obtain the standard results. If we use Eq. (28) and specify a consistent story for each increment of flux change and for the injection and extraction of the associated halo currents from points on the structure, then a correct distribution of currents is obtained.

Experience with this calculational approach shows that short time-scale events (the inductive limit) attempt to preserve the magnetic flux intercepting the structure. Let us consider a small 'tube' of current near the surface of a plasma that has not yet hit the wall. The tube is in mechanical equilibrium. After the tube encounters the conducting structure, the current distribution produced in the structure initially closely approximates the spatial distribution of current in the plasma tube. This is observed in our calculations. Since the tube current is originally force-free and the current in the structure approximately duplicates this distribution, the currents in the structure produce small forces. The spatial distribution of this initial eddy current distribution is usually very different from the resistive distribution obtained by doing a steady state calculation of the injected and extracted halo currents (all forcing voltages $\boldsymbol{b}$ are assumed to be zero). We believe that this resistive distribution of currents produces a greater load per ampere than is found in the inductive limit. In the following results, we are therefore presenting only resistive distributions of current and their resulting forces. A more detailed description of transient currents and forces will be presented at a later time.

5.2. Eddy current calculation of halo currents using the simple kink plasma driver

As an illustrative example, we imagine that a VDE, accompanied by an $m/n = 1/1$ kink instability, has allowed a disrupting plasma to come in contact with a horizontal conducting plate (Fig. 13). Model parameters are chosen so that $R/a = 3.0$, $d/a = 0.1$ and $s/a = 0.10$. The resulting TPF is 2.0.

Sources and sinks of poloidal current are calculated from the model plasma driver at discrete mesh points on the conducting plate and used as input to the eddy current code. The sources and sinks are shown in Fig. 14, where the length of each arrow is proportional to the magnitude of the normal component of the current. A 'resistive' distribution of eddy currents on the conducting plate is then calculated, Fig. 15. In this figure, greater current is associated with a greater width for each arrow and blank elements have current magnitudes that are less than 5% of the maximum current in the plate. The resistive eddy current

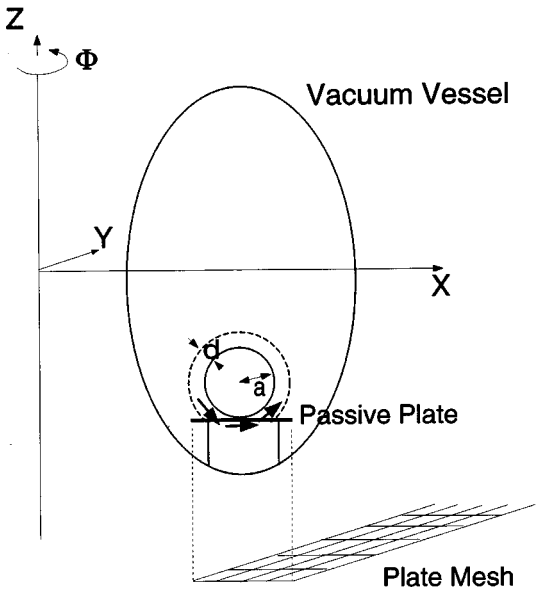

FIG. 13. Simple plasma driver used as current source for the eddy current calculation: an $m/n = 1/1$ kinked plasma is in contact with a flat toroidally continuous conducting plate. At plate mesh points (the nodes of the eddy current simulator), the plasma model supplies sources and sinks of current, $J_Z(X, \phi)$. Although toroidal curvature of the mesh is not apparent in the figure, the mesh is a toroidal ring (e.g., Fig. 14).

distribution shows circulating eddies that extend, necessarily (since the current is divergence-free), beyond the source and sink regions. The eddy current paths are not purely poloidal.

To calculate forces on the plate we assume, in this illustrative example, that the confining poloidal magnetic field is purely vertical and the toroidal field is $B_t \sim 1/R$. Figure 16 shows two perspective views of the forces resulting from the interaction of the resistive eddy current distribution with the toroidal field. We note that there are regions where the force is in the $+\hat{Z}$ direction. This is due to poloidal eddy currents flowing radially in the regions outside of the

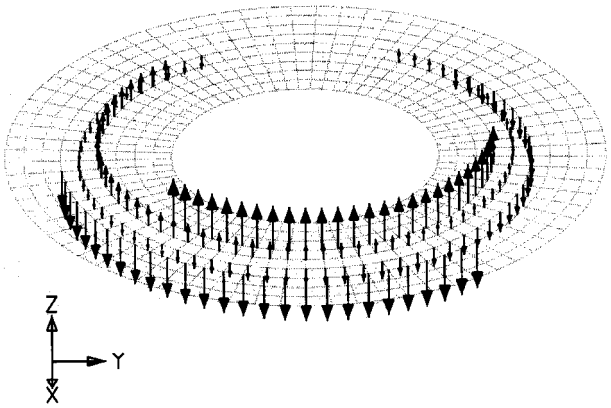

FIG. 14. Perspective view of flat conducting plate, showing the sources and sinks of halo current provided by the $m/n = 1/1$, TPF = 2.0 ($s/a = 0.10$) model plasma driver to the eddy current calculation. The length of each arrow is proportional to the magnitude of J_Z.

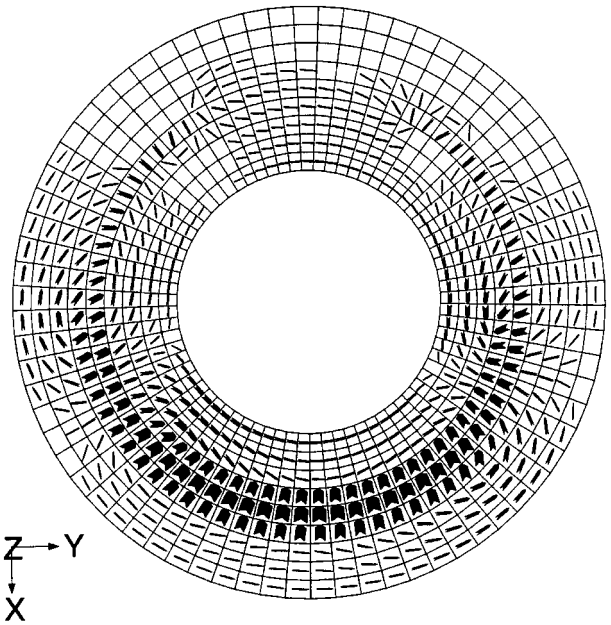

FIG. 15. Calculated resistive distribution of eddy currents on flat conducting plate for $m/n = 1/1$, $s/a = 0.10$, corresponding to a TPF of 2.0. The width of each arrow is proportional to the magnitude of the current.

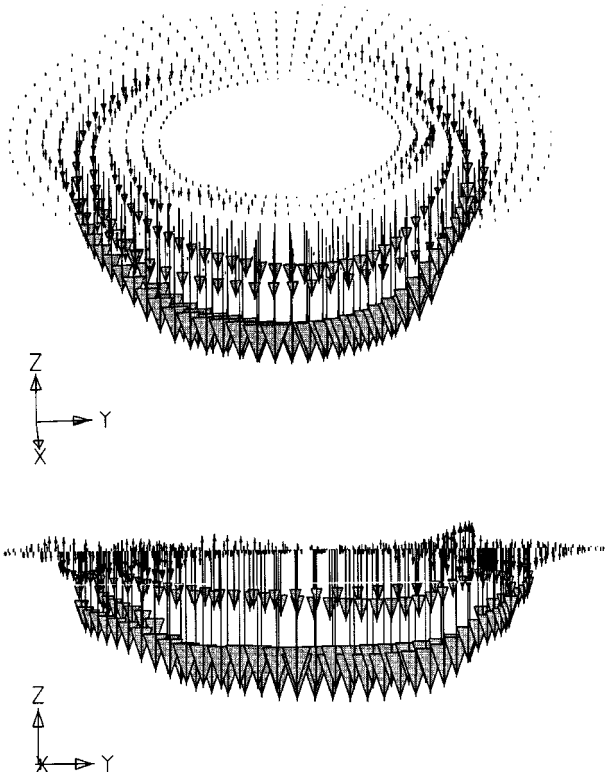

FIG. 16. Calculated forces on flat conducting plate resulting from a resistive current distribution interacting with a toroidal field (perfect $1/X$, in Y direction). Two perspective views are shown. The length of each arrow is proportional to the magnitude of the force.

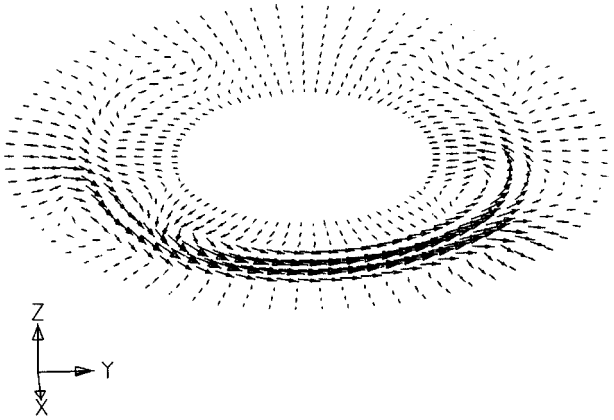

FIG. 17. Forces on flat conducting plate resulting from resistive current distribution interacting with a poloidal field (uniform B_Z). The length of each arrow is proportional to the magnitude of the force.

plasma halo 'footprint'. Figure 17 shows the force distribution due to the interaction of the eddy currents with the poloidal field. In the absence of any toroidal asymmetry, the total force distribution would correspond to a pure torque about the Z axis and a net downward $(-\hat{Z})$ force. Thus, the non-symmetric resistive eddy current distribution leads to a much more complicated force distribution than that which would be predicted by a naïve eddy current model (e.g., one that assumes only a poloidal flow path between the plasma halo and the sinks). It remains for the future to calculate disruption forces using magnetic fields that are self-consistent with the plasma and halo currents.

5.3. Mitigation of TPFs for radial disruptions at low aspect ratio

At conventional aspect ratios (∼3–4, say), the most serious disruptions of vertically elongated plasmas occur when there is a vertical displacement followed by a current quench [2]. This is because a large toroidal current is inductively transferred into the bottom (or top) of the vacuum vessel and interacts with a large poloidal field from a nearby divertor coil. In low aspect ratio tokamaks, however, vertical disruptions are expected to be more benign for two related reasons:

(a) A smaller current in the 'divertor coil' is needed to form an elongated plasma (low aspect ratio plasmas are 'naturally elongated');

(b) Less toroidal current is induced in the bottom (or top) of the vacuum vessel because the vertical drift of the plasma is much slower (since the curvature of the vertical field is very small owing to the absence of divertor coils). Therefore most of the current quench occurs when the plasma is close to the midplane.

At low aspect ratios, radial disruptions can be problematic: to achieve low aspect ratio, the radius of the centre stack, including its structural support, is necessarily small. The interaction of toroidally asymmetric halo currents generated in the central stack casing (CSC) with the external toroidal magnetic field leads to unbalanced loads. The machine must be designed to withstand these loads.

A model plasma driver has been used to estimate halo loads on the CSC in NSTX. NSTX is a device which has an aspect ratio of 1.26, nominal major radius $R = 0.86$ m, minor radius $a = 0.68$ m and elongation $\kappa = 2.0$. The following disruption scenario was assumed: a 1.0 MA plasma has moved radially inward from its nominal equilibrium radius and made contact with the CSC. The equilibrium is shown in Fig. 18. Forty per cent of the initial plasma current is assumed to flow into and out of the CSC at $Z = \pm 0.50$ m with a TPF of 2.0. (That is the net values of all sources and sinks of current sum separately to 400 kA. The sources and sinks of current vary as a function of toroidal angle as $1 - \sin\phi$.)

Using the simple model of the NSTX central stack casing shown in Fig. 18, which has a radius of 0.16 m, we have calculated the resistive distribution of eddy currents and forces on the CSC. The eddy current pattern is shown in Fig. 19. Arrow width represents current magnitude in these plots. In spite of the toroidal asymmetry of the current sources and sinks, the calculated resistive distribution of currents in the CSC (and therefore the calculated forces on the CSC) show a remarkable lack of asymmetry (see plots): on the midplane, midway between the sources and the sinks, the halo current asymmetry is calculated to be only 1.05, compared with 2.00 at $Z = \pm 0.50$ m.

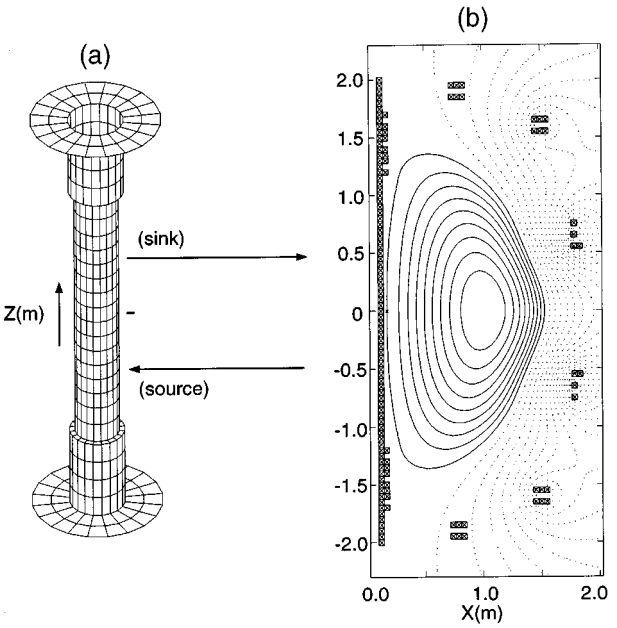

FIG. 18. Model of NSTX central stack casing for calculation of eddy currents. An NSTX plasma equilibrium is also used as the basis for the defining location of current sources and sinks (at $Z = \pm 0.5$ m). In (b) the crossed boxes represent current filaments that model the ohmic and poloidal field coils. The long column of filaments near the inboard edge represents the ohmic 'central stack'. This coil is not in the vacuum but rather is protected by the Inconel cylinder illustrated in (a), this structure being referred to as the central stack casing (CSC).

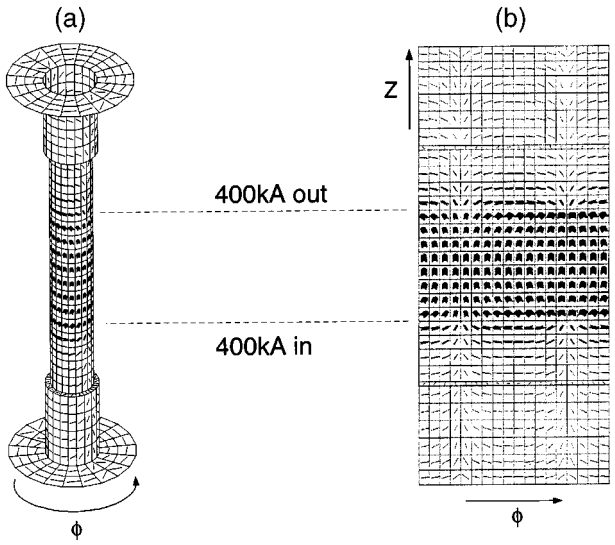

FIG. 19. Resistive solution of halo currents on the CSC. (a) Eddy currents on the cylinder. The width of each arrow is proportional to the magnitude of the current. (b) The same eddy currents on the unwrapped cylinder obtained by making a vertical cut of the CSC.

There appear to be two reasons for this uniformization of the current distribution:

(a) The ratio of the circumference of the CSC to the vertical separation distance between the current sources and sinks is ≈1.0. Therefore, toroidal eddy current paths have a similar impedance to poloidal paths that connect the sources and sinks.

(b) The presence of conductive paths below and above the sinks and sources of the imposed current allow additional smoothing of the resistive distribution. Below, we present the evidence for these propositions.

The calculation of resistive eddy currents was repeated for three simple cylinders similar in shape to the CSC of NSTX. The cylinders have radii equal to 0.16, 0.32 and 0.48 m. The total height of the cylinders is 2.0 m. Defining an aspect ratio, A_c, as the circumference of the conducting cylinder divided by the distance between the source and the sink of current, the aspect ratios of the three cylinders are A_c = 1.0, 2.0 and 3.0. For each case examined, we assumed 1.0 MA of source current, and 1.0 MA of sink current having a toroidal dependence of $1-\sin\phi$, and separated by a distance of 1.0 m. All the models have 20 equal toroidal divisions. Figure 20 illustrates the numerical variation of the vertical component of the current at the point midway between the sources and the sinks. The toroidal peaking factor for the vertical

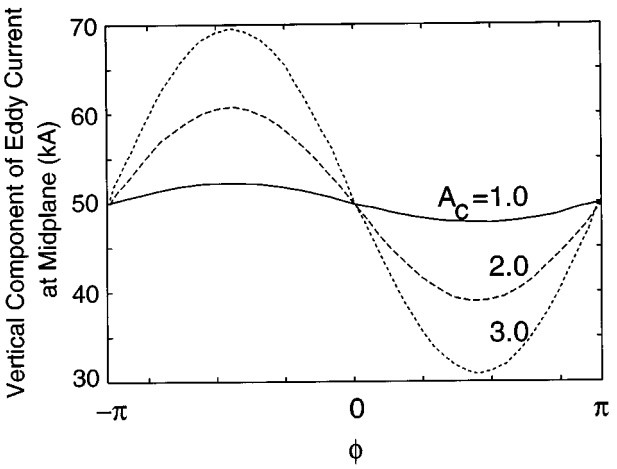

FIG. 20. Toroidal distribution of the vertical component of current along the midplane circumference of the CSC (midway between the sources and the sinks). The different curves correspond to different aspect ratios, A_c, where A_c is the ratio of the midplane circumference of the CSC to the vertical separation between the current sources and the sinks. The value of A_c was varied by changing the radius of the CSC. NSTX corresponds to $A_c = 1.005$.

component of current on the midplane increases from approximately 1.0 for $A_c = 1.0$ to 1.7 for $A_c = 3.0$.

In Fig. 19(b), circulating eddy current paths are seen below and above the line of sources and sinks at $Z = \pm 0.5$ m. The effect of these paths on the toroidal asymmetry of the eddy current distribution was examined by repeating the above calculations after removing the conducting material below and above the line of sources and sinks (i.e. the reduced vertical extent of the cylinders is from $Z = -0.5$ m to $Z = 0.5$ m). Figure 21 presents a direct comparison of the peakedness of the current distribution on the midplane circumference with and without the extra conducting paths.

This example shows substantial mitigation of the TPFs calculated from the resistive eddy current distribution compared with the TPF for the applied current source. The TPFs for the largest forces on the conducting structures depend on the resistive eddy current distribution. These may only be weakly correlated with the TPFs of the plasma current sources.

6. CONCLUSIONS

On the basis of the proposition that the observed toroidal asymmetry of halo currents is mainly due to the deformation of the plasma cross-section caused by the growth of a non-linear kink instability

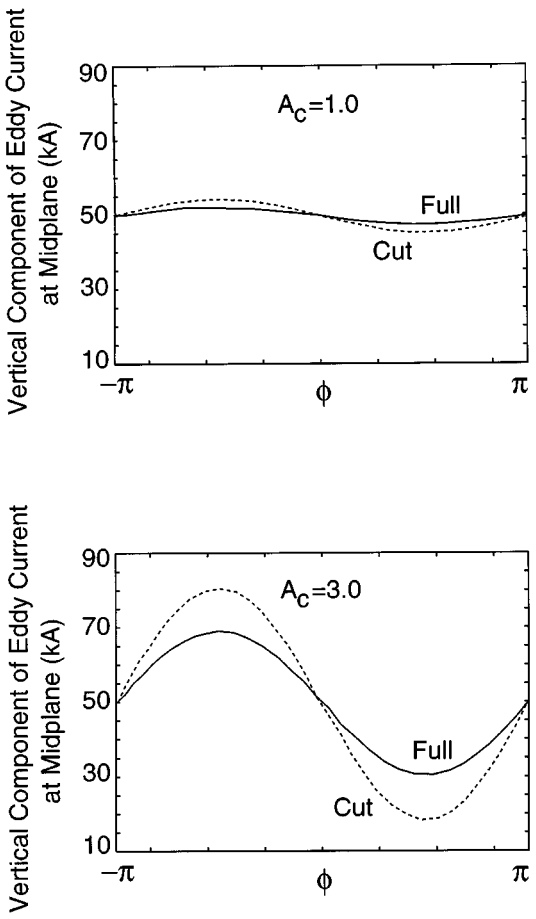

FIG. 21. Comparison of the toroidal distribution of the vertical component of current along the midplane circumference of the CSC with ('full') and without ('cut') conducting material below and above the line of sources and sinks of halo current for $A_c = 1.0$ and $A_c = 3.0$.

during the current quench phase of a plasma disruption, we have presented a simple analytical model of a kink deformed plasma and calculated the TPFs as a function of halo current fraction, I_h/I_p. The dependence of the TPF on I_h/I_p is characterized by a single parameter that measures the plasma deformation caused by the kink instability. For an $m/n = 2/1$ kink instability, this parameter is the surface deformation $\Delta a/a$, which is related to the perturbed elongation of the plasma. For an $m/n = 1/1$ instability, the parameter is s/a, the relative shift of the plasma column. For a given parameter value, the dependence of the TPF on I_h/I_p is roughly hyperbolic, with large peaking factors obtained for low halo current fractions. This dependence appears to agree with experimental observation. For deformations $\Delta a/a \approx 0.3$, or $s/a \approx 0.3$, toroidal peaking factors greater than 2.0 are predicted for halo current fractions of 20%.

For the model to be useful for tokamak design, we need to know the largest expected values of the surface deformations. Numerical experiments can help to answer this question. To date, there have been a number of simulations that predict the amplitude of saturated states of external kink instabilities. These show a range of deformations, depending on the details of the equilibrium profile and of the proximity of conducting walls to the plasma boundary. For realistic values of the conducting wall radius, say $r_w/a \lesssim 1.2$, the maximum deformations so far calculated for $m/n = 2/1$ kink instabilities are $\Delta a/a \approx 0.3$. However, more calculations are needed to extend the calculations to a greater variety of current profiles, and to include the effects of toroidal geometry and finite aspect ratio.

Given that the simple plasma model appears to reproduce, in satisfactory detail, the experimental database of observations of toroidal peaking of halo currents, we have proposed the use of the model as a plasma driver for detailed electromagnetics calculations of eddy currents on 3-D conducting structures. We believe that, from the point of view of tokamak design, it is very important to calculate the distribution of eddy currents correctly, and with present day computing capabilities, coupling such an eddy current code to a detailed 3-D model of a disrupting plasma is not appropriate: the resulting hybrid code would be a very inefficient design tool. Two sample eddy current calculations have been presented that illustrate both the use of the simple plasma driver as a current source for the eddy current calculations and the fact that the results of a realistic eddy current calculation can be significantly different from the results that a naïve model provides.

ACKNOWLEDGEMENTS

We gratefully acknowledge useful discussions with Drs S.C. Jardin and D. Monticello, and helpful remarks by one of the referees. This work was supported by USDOE Contract No. DE-AC020-76-CH03073.

REFERENCES

[1] GRUBER, O., et al., Plasma Phys. Control. Fusion **35** (1993) B191.
[2] SCHULLER, F.C., Plasma Phys. Control. Fusion **37** (1995) A135.
[3] NOLL, P., et al., Fusion Technol. **15** (1989) 259.

[4] REIS, E., et al., in Fusion Engineering (Proc. 12th Symp. Monterey, 1987), Vol. 1, IEEE, New York (1987) 212.
[5] KUGEL, H.W., et al., in Controlled Fusion and Plasma Physics (Proc. 16th Eur. Conf. Venice, 1989), Vol. 13B, Part I, European Physical Society, Geneva (1989) 199.
[6] NEYATANI, Y., YOSHINO, R., ANDO, T., Fusion Technol. **28** (1995) 1634.
[7] STRAIT, E.J., et al., Nucl. Fusion **31** (1991) 527.
[8] GRANETZ, R., et al., Nucl. Fusion **36** (1996) 545.
[9] WESLEY, J.C., in Fusion Energy 1996 (Proc. 16th Int. Conf. Montreal, 1996), Vol. 2, IAEA, Vienna (1997) 971.
[10] PARK, W., et al., Phys. Fluids B **3** (1991) 507.
[11] SAYER, R.O., et al., Nucl. Fusion **33** (1993) 969.
[12] LUKASH, V.E., KHARYUTDINOV, R.R., Plasma Phys. Rep. **22** (1996) 91.
[13] SYKES, A., WESSON, J.A., in Plasma Physics and Controlled Nuclear Fusion Research 1980 (Proc. 8th Int. Conf. Brussels, 1980), Vol. 1, IAEA, Vienna (1981) 237.
[14] DNESTROVSKII, Yu.N., KOSTOMAROV, D.P., Fiz. Plazmy **11** (1985) 1080.
[15] CHANG, Z., et al., Phys. Rev. Lett. **77** (1996) 3553.
[16] POMPHREY, N., et al., in Plasma Physics and Controlled Nuclear Fusion Research 1994 (Proc. 15th Int. Conf. Seville, 1994), Vol. 3, IAEA, Vienna (1995) 251.
[17] WEISSENBURGER, D.W., in Fusion Engineering (Proc. 13th Symp. Knoxville, 1989), Vol. 2, IEEE, New York (1990) 1144.

(Manuscript received 8 August 1997
Final manuscript accepted 16 December 1997)

E-mail address of N. Pomphrey:
pomphrey@pppl.gov

Subject classification: B0, Ti; I2, Ti